A One-dimensional Transient Model of Down-flow Through a Swelling Packed Porous Bed

Martin A. Shadday Jr.

Westinghouse Savannah River Company, Savannah River National Laboratory, Aiken, SC 29808, U.S.A.

Abstract

A transient model of down-flow through an ion exchange column in which the resin swells has been developed. The model is herein described and results are presented. Wall friction can lead to high bed stresses when the resin in columns with high length to diameter ratios swells. These stresses can lead to high and potentially excursive hydraulic pressure drops along a column. A non-dimensional grouping that effectively correlates the final steady-state hydraulic behavior of a column with the resin compressibility, column geometric, and flow parameters has been determined.

Keywords: Ion exchange columns; packed beds; numerical model; transient flow; swelling resin; wall friction

1. Introduction

Many ion exchange resins exhibit considerable shrinking and swelling as they change ionic form, with the potential consequence of significant bed stresses in ion exchange columns. High bed stress reduces bed porosity and increases the hydraulic pressure drop along the column, and it is a consequence of friction between the resin and the column wall that restricts axial expansion of the resin bed. Though this phenomenon has been long recognized, Zenz and Othmer (1960) described a glass ion exchange column that burst due to resin swelling and Kunin (1976) discusses the dangers of swelling induced high stresses in high length to diameter ratio (L/D) laboratory columns, there has not been, to the author's knowledge, a quantitative study of the impact of swelling on ion exchange hydraulics. This paper describes a numerical model of down-flow through an ion exchange column in which the resin swells due to ion exchange reactions. The model predicts the change in bed height, pressure drop, and the axial distributions of bed stress and porosity, as the concentration front moves axially down the column.

The hydraulic performance of ion exchange columns with compressible resins is an area of active research; the goal is generally to develop models for scaling the results of small diameter laboratory tests to large diameter production columns. Fluid drag and wall friction are generally opposing forces on a resin bed. Fluid drag, as a body force, is proportional to the square of the column diameter and the wall friction force is linearly proportional to the diameter. Fluid drag can therefore collapse the bed in a large diameter

column with a sufficiently compressible resin, resulting in an excursive pressure drop, whereas wall friction can support the bed in a small diameter column. This phenomenon is important in scaling from the laboratory to commercial application. Whereas large diameter commercial columns frequently have L/D ratios on the order of unity, small diameter laboratory columns, in which bed length and contact time are preserved, can have very large L/D ratios. There have been a number of studies of the impact of wall friction on steady-flow through ion exchange columns, (Colby *et al*. 1996, Östergren *et al*. 1997 1998 and 1999, Stickel and Fotopoulos 2001, Tiller *et al*. 1972ab, Verhoff and Furjanic 1983, and Willis *et al*. 1974). Verhoff and Furjanic (1983) developed a simple one-dimensional model that clearly demonstrated the effects of column diameter and resin compressibility on pressure drop. Östergren *et al*. (1997, 1998, and 1999) developed a two-dimensional model of steady flow through a compressible bed. Both models dealt solely with elastic compression of the resin, the resin particles could deform under stress but were precluded from moving relative each other. Similar models for the transient hydraulic performance of packed columns with swelling resins are not described in the literature. Marra and Cooney (1973 and 1974) modelled the shrinking and swelling of resin in ion exchange columns, and the impact on concentration profiles. They did not include a force balance in their model, and the predicted swelling was therefore unconstrained.

Pilot scale tests of an ion exchange process to remove ^{137}Cs from high-level radioactive alkaline waste with SuperLig® 644, an elutable organic ground resin, provided the impetus for this investigation. There are plans to remove the ^{137}Cs from the radioactive waste (a legacy of the production of nuclear weapons materials at the U. S. Department of Energy's Hanford Site) for concentration and vitrification in high-level waste glass. During the regeneration step of the process in which the resin is converted from hydrogen to sodium form with 0.25 M sodium hydroxide solution, the resin swells by approximately 30%. The pressure drops during the regeneration steps in small diameter prototypic height column tests increased significantly and were occasionally excursive. While the literature indicated that wall friction was restraining the swelling resin, nothing was found that addressed the swelling and dynamic compression of the resin quantitatively. The model herein described was developed to provide insight into the important phenomena involved in the regeneration process and the impacts on the hydraulic behavior of the column.

2. Model Description

The model scenario is down flow through a packed bed with a constant inlet volume flowrate. The resin is initially in its shrunken form, and an ion solution flows through the column, simultaneously exchanging ions with and swelling the resin. The model tracks the axial motion of the concentration wave fronts of solvent and solid concentrations of the adsorbed ion species, and the resultant local resin swelling and movement of the bed. The transient axial bed stress and porosity distributions and the resultant hydraulic pressure drops are also calculated.

2.1. *Model equations*

The equation set consists of: conservation equations for ion concentrations in the solvent and resin, the solvent continuity equation, an axial force balance on the resin, and constitutive relations for porosity and resin swelling. Hydrodynamic pressure is not a fundamental variable in the model. The pressure drop across the bed is functionally dependent on the axial porosity and flowrate distributions, and can be easily determined at any desired point in the transient. The boundary conditions are zero stress at the top of the bed and constant inlet volume flowrate. The resin is initially in the shrunken state. A zero-flow axial porosity distribution is specified. The initial bed stress and porosity distributions are calculated for steady flow of water through the column. At time zero the inlet flow is switched from water to a solution with a specified ionic concentration that will swell the resin. The transient concludes when the resin concentration is at capacity and the column effluent has the same concentration as the inlet flow.

The rate of ion exchange between the solvent and resin is assumed to be governed by film theory (Geankpolis 1972). With the assumptions that the surface concentration varies linearly with the resin concentration and adsorption ceases when the resin concentration reaches the capacity, the molar adsorption rate is a function of the solvent and resin concentrations. This is a simple rate expression that relates the free stream solvent and resin concentrations with the mass transfer coefficient *k*.

$$\frac{dN_a}{dt} = kA_{srf}\left(C_{slv} - C_{srf}\right) = kA_{srf}C_{slv}\left(1 - \frac{C_{sld}}{C_{cap}}\right) \tag{1}$$

The rate equation for the resin concentration results from dividing by the resin mass.

$$\frac{\partial C_{sld}}{\partial t} = \frac{kA_{srf}}{m_{res}}C_{slv}\left(1 - \frac{C_{sld}}{C_{cap}}\right) \tag{2}$$

The solvent concentration transport equation accounts for both axial convection and adsorption by the resin. Because there is a one-for-one ion exchange between the solvent and resin, only one species need be tracked, in this case the adsorbed ions. The two simple resin and solvent concentration rate equations are adequate approximations for this model, in which the primary objective is the impact of swelling on hydraulic behavior. In addition to the particle geometry, the two parameters that govern the ion exchange kinetics are the mass transfer coefficient and the resin capacity. The terms for the ion adsorption rates in the two concentration rate equations differ because the solvent molar concentration is defined on a volume basis and the resin molar concentration is defined on a mass basis.

$$\frac{\partial C_{slv}}{\partial t} + \frac{\partial\left(vC_{slv}\right)}{\partial z} = -\frac{kA_{srf}}{V_{slv}}C_{slv}\left(1 - \frac{C_{sld}}{C_{cap}}\right) \tag{3}$$

As the resin swells, solvent accumulates in the increasing particle interstitial volume and in the increasing pore volume. The pore porosity is assumed to be a constant in this analysis and therefore independent of the bed stress. The pore volume is directly proportional to the resin volume and therefore increases as the resin swells. The concentration of the pore liquid is assumed to be the same as that of the interstitial liquid. The pore porosity impacts the dry mass of resin and the solvent holdup during swelling. It does not directly affect the ion exchange rate in this simple model.

The interstitial volume is a function of porosity as well as resin swelling. With increasing bed stress, the local porosity can decrease while the resin volume increases. Equation (4) is the solvent continuity equation. The solvent density is assumed to be a constant, independent of adsorbed ion concentration. The term on the left side of the equation is the convective term, and the two terms on the right side are respectively the interstitial and pore volume accumulation terms.

$$V\frac{\partial v}{\partial z} = -\frac{\partial(\varepsilon V)}{\partial t} - \varepsilon_p \frac{\partial}{\partial t}\left[(1-\varepsilon)V\right] \tag{4}$$

The bed stress distribution is determined from a force balance on the resin, using the Janssen approach (Nedderman 1982) of differential slices. The net force acting on an axial segment of a column is the sum of the gravitational, viscous drag, and wall friction forces. These forces are represented respectively by the three terms on the right side of equation 5. The viscous drag force is calculated with the Kozeny-Carman equation. The direction of the wall friction force changes during the transient. It initially opposes the gravitational and viscous forces, but as the resin swells, pushing the resin above the swelling zone vertically upward, the direction of the wall friction changes to oppose the motion of the resin. The coefficient *k'* in the wall friction term is the ratio of the radial to axial stress components. This term is necessary because only the axial component of bed stress is a variable in this one-dimensional model, and the wall friction force is a function of normal component of stress. The wall friction term is elaborated on in the next subsection.

$$\frac{\partial \sigma}{\partial z} = \Delta\rho(1-\varepsilon) + f\frac{(1-\varepsilon)^2 v}{\varepsilon^3} \pm \omega\sigma \tag{5}$$

where: $\Delta\rho = (\rho_s - \rho_l)(1-\varepsilon_p)g$

and $f = \dfrac{180\mu}{\Phi^2 d_p^2}$ & $\omega = \dfrac{4\mu' k'}{D}$

Equation (6) is the constitutive relation between porosity and the bed stress (Verhoff and Furjanic 1983). There are three mechanisms for porosity reduction within a particle bed: deformation of the particle shape under stress to fill interstitial void, rearrangement of the particles to a more dense packing, and the filling of void with fines produced by particle breakup. The latter two irreversible mechanisms are not addressed in this model. Only

elastic particle deformation is considered. Fines production can be eliminated with sufficiently robust spherical particles, and the rearrangement of particles can be mitigated by appropriately consolidating the bed prior to operation. This is done by alternately loading the bed to at least the highest stress level expected and unloading until the bed responds reversibly (Östergren *et al*. 1998). The resin compressibility is determined empirically with uniaxial compression tests (Verhoff and Furjanic 1983).

$$\varepsilon = \frac{\varepsilon_0}{1+\alpha\sigma} \tag{6}$$

The resin is assumed to swell linearly with the adsorbed ion concentration. The compressibility α in equation 6 is a measure of the bed elastic compressibility and does not reflect the bulk compressibility of the resin material. The bed compresses by deformation of the resin particles to fill void. The volumes of the resin particles are assumed to be independent of applied stress and are only functions of swelling.

$$V_{res} = V_{h_2}\left(1+\frac{C_{sld}}{C_{cap}}f_{swl}\right) \tag{7}$$

The resin particle diameter and skeletal density change as a consequence of swelling, equations (8) and (9).

$$d_p = d_{p0}\left(1+\frac{C_{sld}}{C_{cap}}f_{swl}\right)^{1/3} \tag{8}$$

$$\rho_s = \frac{\rho_{s0}}{1+\frac{C_{sld}}{C_{cap}}f_{swl}} \tag{9}$$

The hydrodynamic pressure is not a fundamental variable in this model. The pressure drop across the column can be determined at any time by integrating the Kozeny-Carman equation (10) over the length of the column.

$$\frac{\partial P}{\partial z} = \frac{180\mu}{\Phi^2 d_p^2}\frac{(1-\varepsilon)^2}{\varepsilon^3}v \tag{10}$$

2.2. *Numerical model*

A one-dimensional finite-difference scheme is used to model the flow through the column. To accommodate the swelling and axial translation of the resin bed, a deformable mesh is utilized. The bed is divided into a discrete number of stacked horizontal slice control volumes. The control volume thicknesses are initially uniform.

Resin does not cross the control surfaces, and therefore the resin mass within a control volume is invariant. During the flow transient, the individual control volume thicknesses change as the resin swells and the porosity decreases due to compression. The control volumes also translate axially in response to the bulk expansion of the bed.

The finite-difference forms of the governing equations are derived with the control volume approach rather than finite-differencing the differential equations directly. This assures internal consistency within the model. The equations are formulated implicitly. The model marches axially down the column, treating each incremental control volume sequentially, and marches forward in time. Six simultaneous equations are solved for each control volume: the resin and solvent adsorbed ion concentration equations, the axial force balance, the solvent continuity equation, the compressibility constitutive equation, and the resin swelling constitutive equation. These are equations 11 through 16 respectively. The variables solved for are: the solvent and resin adsorbed ion concentrations, volume flowrates, axial components of bed stress, porosities, and axial thicknesses of the incremental control volumes. The following equations are for the i^{th} control volume, and the superscripts *n* and *n+1* indicate variable values at the old and new time-steps respectively. The volume flowrates and bed stresses are defined at the axial boundaries of the control volumes, and the concentrations and porosities are volume averaged values for the control volumes.

$$\frac{m_{res_i}}{\Delta t}\left(C_{sld_i}^{n+1}-C_{sld_i}^{n}\right)=\frac{6kA_{cs}\Delta z_i^{n+1}\left(1-\varepsilon_i^{n+1}\right)}{d_{p0}\left(1+\frac{C_{sld_i}^{n+1}}{C_{cap}}f_{swl}\right)^{1/3}}C_{slv_i}^{n+1}\left(1-\frac{C_{sld_i}^{n+1}}{C_{cap}}\right) \tag{11}$$

$$\left[\varepsilon_i^{n+1}+\varepsilon_p\left(1-\varepsilon_i^{n+1}\right)\right]A_{cs}\Delta z_i^{n+1}\left(\frac{C_{slv_i}^{n+1}-C_{slv_i}^{n}}{\Delta t}\right)=\dot{Q}_{i-1}^{n+1}C_{slv_{i-1}}^{n+1}-\dot{Q}_i^{n+1}C_{slv_i}^{n+1}- \tag{12}$$
$$\frac{6kA_{cs}\Delta z_i^{n+1}\left(1-\varepsilon_i^{n+1}\right)}{d_{p0}\left(1+\frac{C_{sld_i}^{n+1}}{C_{cap}}f_{swl}\right)^{1/3}}C_{slv_i}^{n+1}\left(1-\frac{C_{sld_i}^{n+1}}{C_{cap}}\right)$$

$$\frac{\sigma_i^{n+1}-\sigma_{i-1}^{n+1}}{\Delta z_i^{n+1}}=\left(\frac{\rho_{s0}}{1+\frac{C_{sld_i}^{n+1}}{C_{cap}}f_{swl}}-\rho_l\right)\left(1-\varepsilon_p\right)g\left(1-\varepsilon_i^{n+1}\right)+ \tag{13}$$
$$\frac{90\mu}{A_{cs}\Phi^2}\frac{\left(1-\varepsilon_i^{n+1}\right)^2}{\left(\varepsilon_i^{n+1}\right)^3}\frac{\dot{Q}_i^{n+1}+\dot{Q}_{i-1}^{n+1}}{d_{p0}^2\left(1+\frac{C_{sld_i}^{n+1}}{C_{cap}}f_{swl}\right)^{2/3}}\mp\frac{2\mu'k'}{D}\left(\sigma_i^{n+1}+\sigma_{i-1}^{n+1}\right)$$

$$\dot{Q}_i^{n+1} - \dot{Q}_{i-1}^{n+1} + \frac{A_{cs}}{\Delta t}\left\{\left[\varepsilon_i^{n+1} + \varepsilon_p\left(1-\varepsilon_i^{n+1}\right)\right]\left(\Delta z_i^{n+1} - \Delta z_i^{n}\right) + \Delta z_i^{n+1}\left(1-\varepsilon_p\right)\left(\varepsilon_i^{n+1} - \varepsilon_i^{n}\right)\right\} = 0 \quad (14)$$

$$\left[2 + \alpha\left(\sigma_i^{n+1} + \sigma_{i-1}^{n+1}\right)\right]\varepsilon_i^{n+1} - 2\varepsilon_0 = 0 \quad (15)$$

$$\left(1-\varepsilon_i^{n+1}\right)A_{cs}\Delta z_i^{n+1} = V_0\left(1 + \frac{C_{sld_i}^{n+1}}{C_{cap}} f_{swl}\right) \quad (16)$$

The third term on the right-hand side of equation (13) accounts for wall friction. With steady-state down flow through a compressible resin, this term is normally negative, with the wall friction opposing the compression due to fluid drag and the weight of the resin. Resin swelling is assumed to occur in the region of the bed where ion adsorption is taking place. The resin above the expansion region is pushed upward. Wall friction opposes the motion of the resin and therefore the sign of the wall friction term in the force balance is positive for this region of the bed.

As noted earlier, the coefficient *k'* in the wall friction term is the ratio of the radial to axial stress components. In situations where the resin is subjected to an axial stress such as fluid drag or resin pushing from above or below, *k'* is a function of the angle of internal friction. Figure 1 shows Mohr's circle for the case where the axial and radial stress components are respectively the major and minor principal stresses (McCabe and Smith 1976). The point of tangency to Mohr's circle of a line running through the origin is the state of stress in which the ratio of the shear to normal stress is a maximum. The angle that this line forms with the horizontal axis is the angle of internal friction, which is a property of the granular material. The tangent of this angle is the coefficient of friction between two layers of particles. The angle of internal friction is determined by measuring the required force to shear two layers of particles for various values of an applied normal stress. Equation 17 is the ratio of the radial to axial stresses as a function of the angle of internal friction, and it is obviously less than unity.

$$k' = \frac{1-\sin\alpha_{if}}{1+\sin\alpha_{if}} \quad (17)$$

The resin swelling is isotropic and the resultant state of stress due to the constraining column wall and the resin above and below is essentially pure biaxial compression. The above described theory does not apply, and the radial and axial components of stress are essentially equal with *k'* close to unity. In the model, *k'* has the value defined by equation 17 except where the resin is undergoing swelling. In this region, *k'* varies from the equation 17 property value to unity, at the point where the swelling rate is a maximum.

The six simultaneous equations for each incremental control volume are solved by Newton's method. The inlet volume flowrate and solvent concentration are specified and

the stress at the top of the bed is zero. The initial resin concentration of adsorbed ions is also zero.

2.3. *Resin properties*

The resin properties used in the model are those of SuperLig® 644 resin. It is stored in sodium form, which is the swollen form of the resin, in deionized water, and this is the form in which physical properties were generally measured. The solvent is 0.25 M sodium hydroxide solution. The resin and solvent properties are listed in Table 1.

The mean particle diameter and shape factor were determined from the results of steady-state hydraulic flow tests with various packed bed particle size distributions. The resin compressibility in the sodium form was measured in a uniaxial compression device very similar to that described by Verhoff and Furjanic (1983). Resin, submerged in water, was compressed in a cylinder by a porous piston, see fig. 2. The position of and the applied force on the piston, and the resin stress at the bottom of the cylinder were measured. Equation 18 is an expression for the product of the coefficient of wall friction and the ratio of the radial to axial stress components as a function of the top and bottom resin stresses. Equation 19 is the expression for the resin compressibility. The resin was consolidated by repeatedly loading and unloading the piston until the compression of the resin was repeatable.

$$\mu' k' = -\frac{D}{4H} \ln\left(\frac{\sigma_B}{\sigma_T}\right) \tag{18}$$

$$\alpha = \frac{1}{\sigma_T} \frac{e^{-\omega(H_0 - H)\left(\frac{1-\varepsilon_0}{\varepsilon_0}\right)} - 1}{e^{-\omega H} - e^{-\omega(H_0 - H)\left(\frac{1-\varepsilon_0}{\varepsilon_0}\right)}} \tag{19}$$

where: $$\omega = \frac{4\mu' k'}{D}$$

The coefficient of wall friction and the angle of internal friction were measured by Jenike & Johanson Inc., a company that specializes in testing granular materials.

Values for the mass transfer coefficient and the resin capacity were evaluated from two observations: an isolated resin particle swells in a couple of minutes when submerged in caustic solution, and the concentration wave front of quarter molar sodium solution moves through resin in hydrogen form at 1.07 cm/min when the superficial velocity is 7.2 cm/min. The mass transfer coefficient is determined by integrating eqn. 2, the rate equation for resin concentration, and assuming the resin concentration is 95% of the resin capacity after two minutes. The particle diameter is assumed to be 313.0 μm. The resin capacity is calculated with the assumption the resin concentration behind the

concentration wave front is at capacity and the solvent concentration is the inlet value. The bed porosity is assumed to be 0.38.

3. Results and Discussion

Figures 3 through 10 show results for flow through a column with an inside diameter of 0.1 m and an initial column height of 0.7 m. The inlet flowrate corresponds to a superficial velocity of 0.0012 m/s (7.2 cm/min). The axial profiles of normalized solvent and resin ion concentrations are shown in fig. 3 at four different times during the transient. The two concentrations are normalized with the inlet solvent concentration and the resin ion capacity respectively. The concentration wave fronts are sharp and their shapes do not change appreciably as they travel down the column. Figure 4 shows the axial profiles of volume flowrate at the same four times in the transient. The flowrates are normalized with the inlet flowrate. The flowrate decreases as the resin swells due to solvent accumulation in the increasing interstitial and pore volumes. Downstream of the concentration front, the flowrate increases due to compression of the resin by upstream swelling resin and axial expansion of the bed that is constrained by wall friction. The initial reduction in axial flowrate results in a decrease in the column pressure drop. Figure 5 shows the axial bed stress profiles and fig. 6 shows the axial porosity profiles at four intermediate times during the transient and at the end. The peak bed stress and minimum porosity occur spatially where the resin is swelling, and at the conclusion of the transient at the column bottom. Figure 7 shows the transient bed height. Though the resin swells by 30 %, because of wall friction the bed height increases by only 23 %. Figure 8 shows the transient bottom bed stress and effluent concentration of absorbed ions. The peak stress occurs while the resin at the bottom of the column is swelling, and there is some relaxation once the swelling concludes. This relaxation is due to the change in value of the ratio of principal stresses k' from unity for swelling biaxial compression to the value for uniaxial compression. Figure 9 shows the transient pressure drop along the column. The initial decrease in pressure drop is due to the drop in flowrate through the column caused by the resin at the top of the column swelling, see fig. 4. After the initial decrease, the column pressure drop increases due to: the increase in height of the column, the increase in height averaged flowrate as the region of swelling proceeds down the column, and the reduction in porosity due to swelling and wall friction induced compression. Figure 10 shows the initial, final, and three intermediate column axial hydraulic pressure drop profiles. The axial distance above the column bottom is normalized with the initial column height, and the axial expansion of the column is clearly evident. The pressure drop profile is initially linear, as one expects for steady flow through a column with no axial variations in mean particle size and bed porosity. As the column expands, the pressure drop gradient in approximately the upper third of the column decreases slightly because the increase in mean particle diameter more than compensates for the small reduction in porosity. The porosity reduction is dominant in the lower half of the column late in the transient, resulting in significant increases in pressure drop gradient.

Figures 11 through 13 show transient plots of normalized bed height, bottom stress, and hydraulic pressure drop respectively for flow through columns with four different initial height to diameter ratios (L/D). In all cases the column diameter is 0.1 m and the inlet flowrate is such that the superficial velocity is 0.0012 m/s. The three calculated variables are normalized with the initial values, and the elapsed time is normalized with the time to steady-state. The threshold L/D ratio, for which constrained swelling in the lower part of the column starts to significantly impact the bed stress and hydraulic pressure drop, is approximately three.

Figures 14 through 16 show the normalized final column heights, bottom bed stresses, and pressure drops respectively as functions of the resin compressibility. Results are shown for three values of the L/D ratio: 5.0, 6.0, and 7.0. The dimensionless parameter that correlates the final steady-state column hydraulic behavior with the resin compressibility, the solvent superficial velocity and viscosity, the column diameter, and the resin particle diameter is:

$$\overline{\alpha} = \frac{\alpha V_{sf} D \mu}{D_p^2} \tag{20}$$

In figs. 14 through 16, the reference values of the superficial velocity, viscosity, column diameter, and particle diameter are respectively 0.0012 m/s, 0.001007 Pa-s, 0.1 m, and 313 μm. The ability of $\overline{\alpha}$ to correlate the column hydraulic behavior with these parameters is demonstrated by the diamond symbols in the three figures. They represent model results in which the parameters vary from the reference values. The superficial velocity varies between 0.0006 and 0.0018 m/s, the column diameter varies between 0.05 and 0.15 m, the viscosity varies between 0.001 and 0.0015 Pa-s, and the particle diameters vary between 250.0 and 376.0 μm. The three figures clearly show the potential for excursive hydraulic behavior with excessively compressible resin in columns with unfavorable geometries.

4. Conclusions

A transient numerical model of down-flow through an ion-exchange column, filled with a swelling resin, has been developed, and the model results provide considerable insight into the coupled phenomena taking place and the impact on column hydraulics. With an L/D ratio below approximately 3.0, wall friction retardation of the bed axial expansion is negligible. With higher L/D columns, the resin in the lower part of the column cannot accommodate swelling by expanding axially, and therefore high bed stress distorts the shape of the particles and reduces the local bed porosity. The porosity reduction has an adverse impact on column hydraulic behavior. This clearly demonstrates the inadvisability of small diameter test columns, with a shrinking and swelling resin, in which bed height is preserved. The L/D ratio is clearly important for predicting hydraulic behavior.

The dimensionless groupings $\overline{\alpha}$ and L/D effectively correlate the final steady-state hydraulic behavior with respect to most of the relevant flow, column geometry, and resin property parameters. They also correlate the pressure drop and axial bed compression due to steady-state flow through a compressible packed bed, if the pressure drop and bed compression are normalized with the zero compressibility values. Figure 17 shows the axial bed compression and pressure drop for steady flow through a column with a compressible resin. Results are shown for L/D values of 5.0, 6.0, and 7.0. A comparison of these results with those in figs. 14 through 16, which show the influence of compressibility on the final hydraulic parameters following swelling, clearly demonstrates that an excursive pressure drop will occur during or following a swelling transient at a much lower value of $\overline{\alpha}$ than for steady flow. With an L/D ratio of 7.0, the pressure drop becomes excursive for flow through a swelling resin with $\overline{\alpha}$ approximately equal to 1.0×10^{-5}, whereas with steady flow through a non-swelling resin the critical value of $\overline{\alpha}$ is approximately 7.0×10^{-5}. The adverse consequence of excessive resin compressibility will first appear during a swelling transient.

A significant assumption in this model is the bed responds elastically to stress. No movement of particles relative to each other is allowed. This assumption is necessary because particle movement that alters the packing would increase the complexity of the problem enormously, essentially to the point of intractability. For this assumption to be reasonable for an actual ion exchange column, the resin bed must be consolidated such that the particle packing is very efficient. This is achieved by alternately loading the bed to the maximum expected stress level and subsequently unloading the bed for a number of cycles until the axial compression and expansion response of the bed is repeatable. This is probably best done hydraulically because an effective body force is applied, rather than mechanically applying axial stress with a piston. In high L/D columns the applied stress is attenuated axially by wall friction. For high L/D columns with a swelling resin, consolidation by alternately swelling and shrinking the resin could be the only effective method of achieving the high stress levels near the bed bottom that result from swelling. As long as the particles remain intact, it is reasonable to expect the bed to approach, with repeated cycles, an ultimate consolidation state. The resin at the bottom of the column would be significantly more consolidated than the resin at the top, and therefore the no-load axial porosity distribution would be nonlinear.

The basis for the model treatment of k' for the swelling resin is a heuristic argument, though the relaxation of the bottom bed stress at the completion of the transient has been observed in column tests. Quality experimental data to confirm the manner in which the model treats wall friction while the resin is swelling is a priority need. This is certainly the most speculative aspect of the model. A more rigorous treatment will require a multi-dimensional model such as that of Östergren *et al*. (1997, 1998, and 1999).

Acknowledgement

The information contained in this paper was developed during the course of work done under contract No. DE-AC09-96SR18500 with the U. S. Department of Energy.

Nomenclature

A_{cs}	column cross-sectional area (m^2)
A_{srf}	particle surface area (m^2)
C_{cap}	resin molar concentration capacity (*mols/kg*)
C_{sld}	resin molar concentration (*mols/kg*)
C_{slv}	solvent molar concentration ($mols/m^3$)
C_{srf}	solvent molar concentration at particle surface ($mols/m^3$)
d_p	particle diameter (*m*)
D	column diameter (*m*)
f_{swl}	resin swell factor
g	gravitational acceleration (m/s^2)
H	column height (*m*)
k	mass transfer coefficient (*m/s*)
k'	ratio of radial to axial stress components
m_{res}	resin dry mass (*kg*)
N_a	mols of adsorbed ions (*mols*)
P	pressure (*Pa*)
$\dot{Q}$	volume flowrate (m^3/s)
t	time (*s*)
v, V_{sf}	superficial velocity (*m/s*)
V	volume (m^3)
α	resin compressibility (Pa^{-1})
$\overline{\alpha}$	dimensionless parameter, eqn. 20
α_{if}	angle of internal friction
ε	bed porosity
ε_0	reference porosity
ε_p	pore porosity
μ	solvent viscosity (*Pa-s*)
μ'	coefficient of wall friction
ρ_l	solvent density (kg/m^3)
ρ_s	resin skeletal density (kg/m^3)
σ	axial component of bed stress (*Pa*)
Φ	resin particle shape factor

References

Colby, C. B., O'Neill, B. K., Middelberg, A. P. J. (1996) A Modified Version of the Volume-Averaged Contuum Theory to Predict Pressure Drop across Compressible Beds of Sepharose Big-Beads SP. *Biotechnol. Prog*., **12**, 92-99.

Denny, P. J. (2002) Compaction Equations: a Comparison of the Heckel and Kawakita Equations. *Powder Technology*, **127**, 162-172.

Geankoplis, C. J. (1972) Mass Transport Phenomena, pp. 299-301, Holt Rinehart and Winston Inc., New York.

Jiang, Y., Khadilkar, M. R., Al-Dahhan, M. H., Dudukovic, M. P. (2000) Single Phase Flow Modeling in Packed Beds: Discrete Cell Approach revisited. *Chemical Engineering Science*, **55**, 1829-1844.

Kunin, R. (1976) Safety Practices in Ion Exchange Technology. *Amber-Hi-Lites*, no. 153, Rohm and Haas Company.

Marra, R. A. and Cooney, D. O. (1973) An Equilibrium Theory for Sorption Accompanied by Sorbent Bed Shrinking or Swelling. *AIChE Journal*, vol. 19, no. 1, 181-183.

Marra, R. A. and Cooney, D. O. (1974) The Effects of Sorbent Shrinking and Swelling on Fixed-Bed Sorption Operations. *AIChE Symposium Series, Adsorption and Ion Exchange*, vol. 71, no. 152, 148-156.

McCabe, W. L. and Smith, J. C. (1976) Unit Operations of Chemical Engineering, pp. 809-816. McGraw-Hill Book Company, New York.

Nedderman, R. M. (1982) The Theoretical Prediction of Stress Distributions in Hoppers. *Trans. Inst. Chem. Eng*., **60**, 259-275.

Östergren, K. C. E. and Trägårdh, C. (1997) Numerical Study of Two-Dimensional Compaction, Flow, and Dispersion in a Chromatographic Column. *Numerical Heat Transfer*, part A, **32**, 247-265.

Östergren, K. C. E., Trägårdh, C., Enstad, G. G., Mosby, J. (1998) Deformation of a Chromatic Bed during Steady-State Liquid Flow. *AIChE Journal*, vol. 44, 1, 2-12.

Östergren, K. C. E. and Trägårdh, C. (1999) Modelling and Analysis of Axial Flow Through and Compression of a Non-rigid Chromatographic Bed. *Chemical Engineering Journal*, **72**, 153-161.

Stickel, J. J. and Fotopoulos, A. (2001) Pressure-Flow Relationships for Packed Beds of Compressible Chromatography Media at Laboratory and Production Scale. *Biotechnol. Prog*., **17**, 744-751.

Tiller, F. M., Stewart, H. Jr., Lu, W. (1972)a The Role of Porosity in Filtration VII: Effect of Side-Wall Friction in Compression-Permeability Cells. *AIChE Journal*, vol. 18, no. 1.

Tiller, F. M. and Lu, W. (1972)b The Role of Porosity in Filtration VIII: Cake Nonuniformity in Compression-Permeability Cells. *AIChE Journal*, vol. 18, no. 3.

Verhoff, F. H. and Furjanic, J. J. Jr. (1983) Compressible Packed Bed Fluid Dynamics with Application to a Glucose Isomerase Reactor. *Ind. Eng. Chem. Process Des. Dev.*, **22**, 192-198.

Zenz, F. A. and Othmer, D. F. (1960) Fluidization and Fluid-Particle Systems, pp. 74-80. Reinhold Publishing Corp., New York.

Tables and Figures:

Resin skeletal density	1131.0 kg/m^3
Pore porosity	0.7
Coefficient of wall friction	0.28
Ratio of principal stresses	0.42
Resin compressibility	2.2×10^{-6} Pa^{-1}
Particle diameter	313.0 μm
Resin swell factor	0.3
Resin ion capacity	5.805 mols/kg
Mass transfer coefficient	1.33×10^{-5} m/s
Inlet solvent concentration	250.0 mols/m^3
Solvent density	1000.0 kg/m^3
Solvent viscosity	0.001007 Pa-s

Table 1: Resin in swollen form and solvent properties

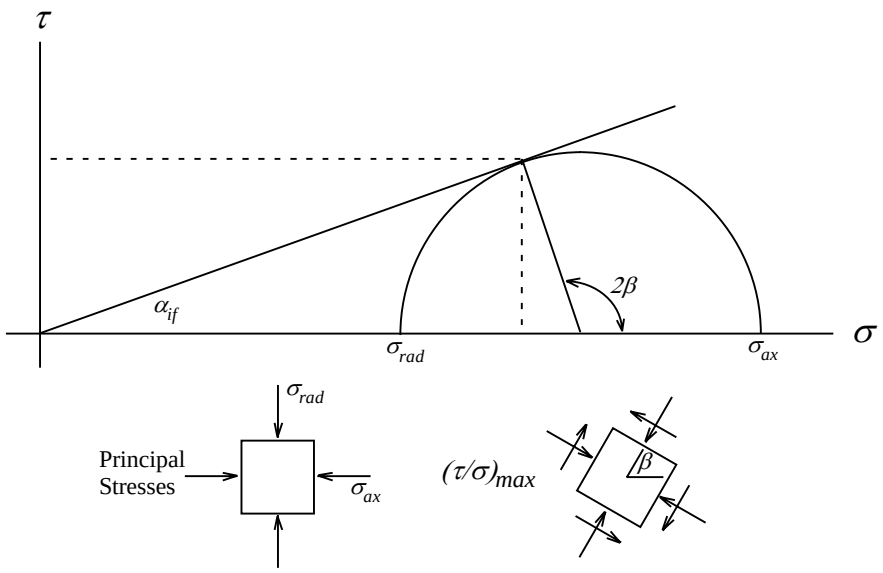

Fig. 1: Mohr's circle for a granular material subjected to an axial stress in a column. The angle of internal friction α_{if} is determined from the maximum value of the shear to normal stress ratio.

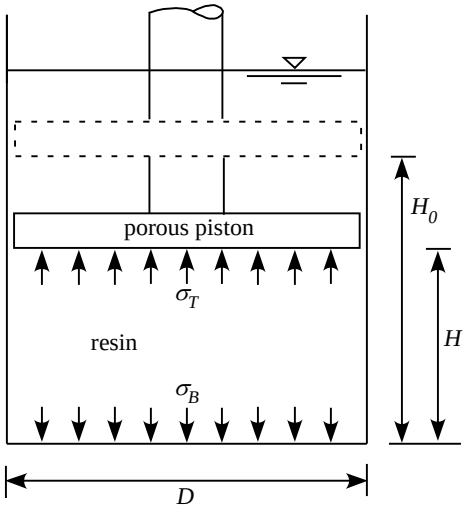

Fig. 2: Schematic of the bed compressibility test apparatus.

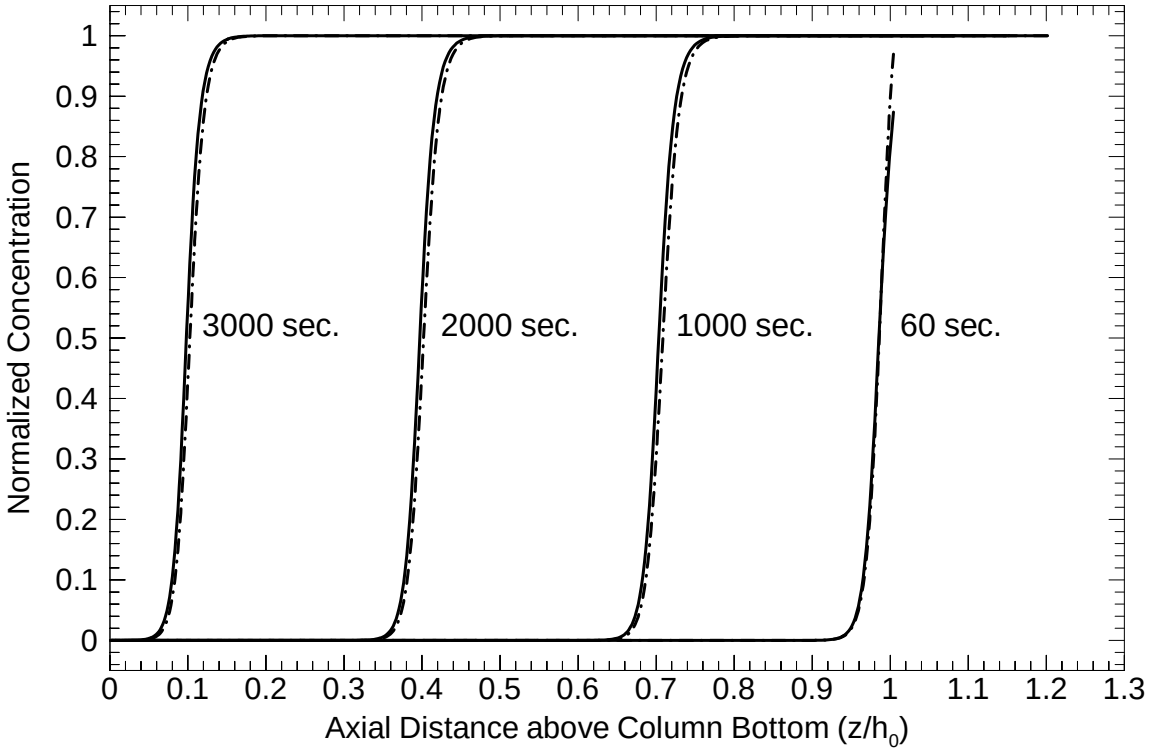

Fig. 3: Axial distributions of the normalized solvent (dashed line) and resin (solid line) adsorbed ion concentrations at four elapsed times in the transient.

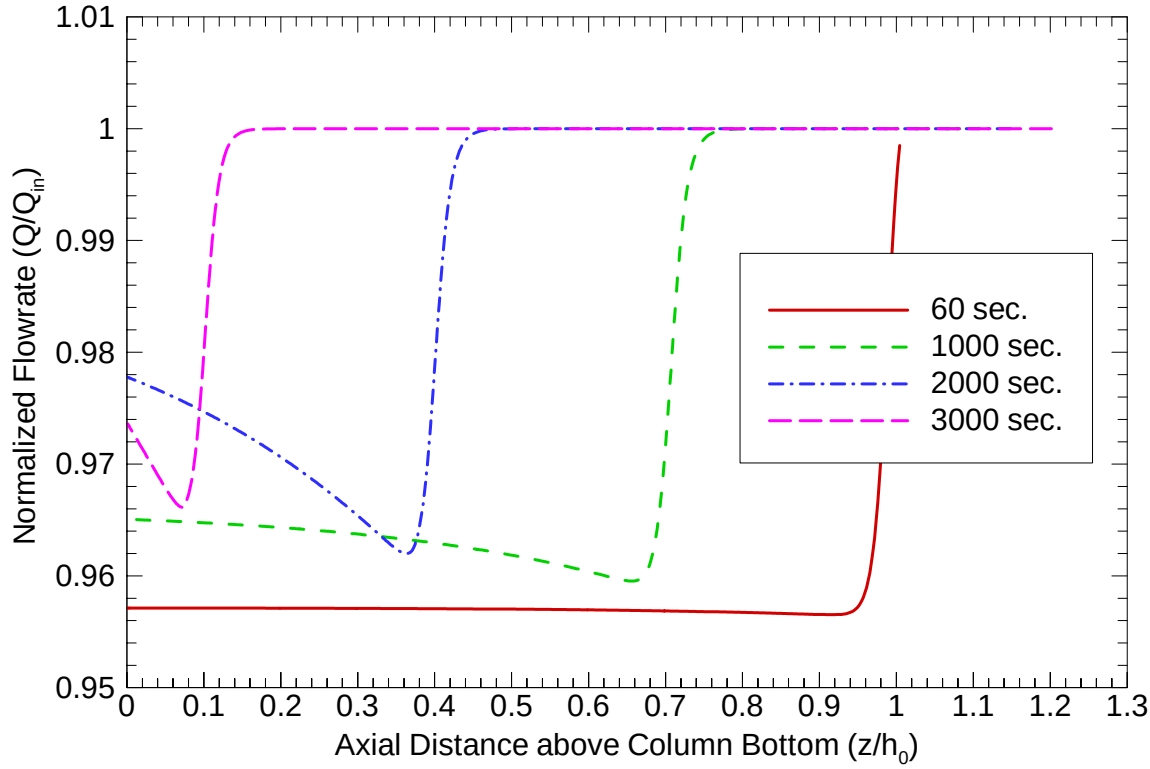

Fig. 4: Axial distributions of volume normalized flowrate at four elapsed times in the transient.

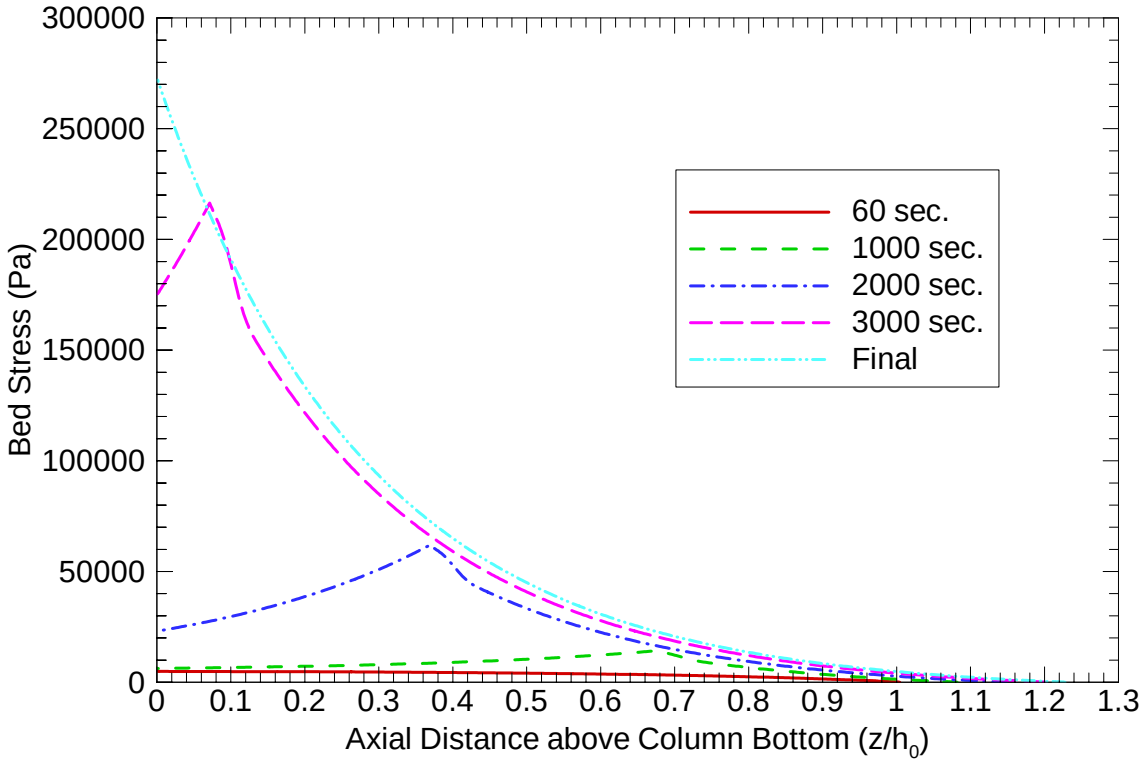

Fig. 5: Axial profiles of bed stress at five elapsed times during the transient.

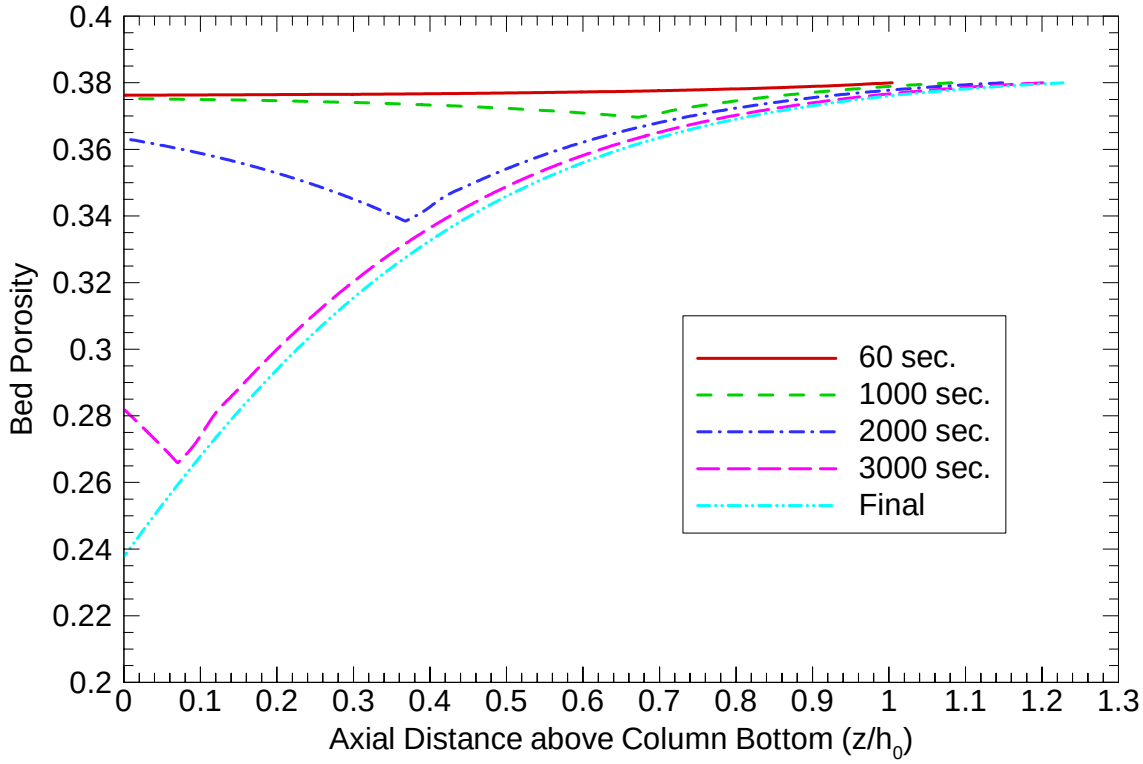

Fig. 6: Axial profiles of bed porosity at five elapsed times during the transient.

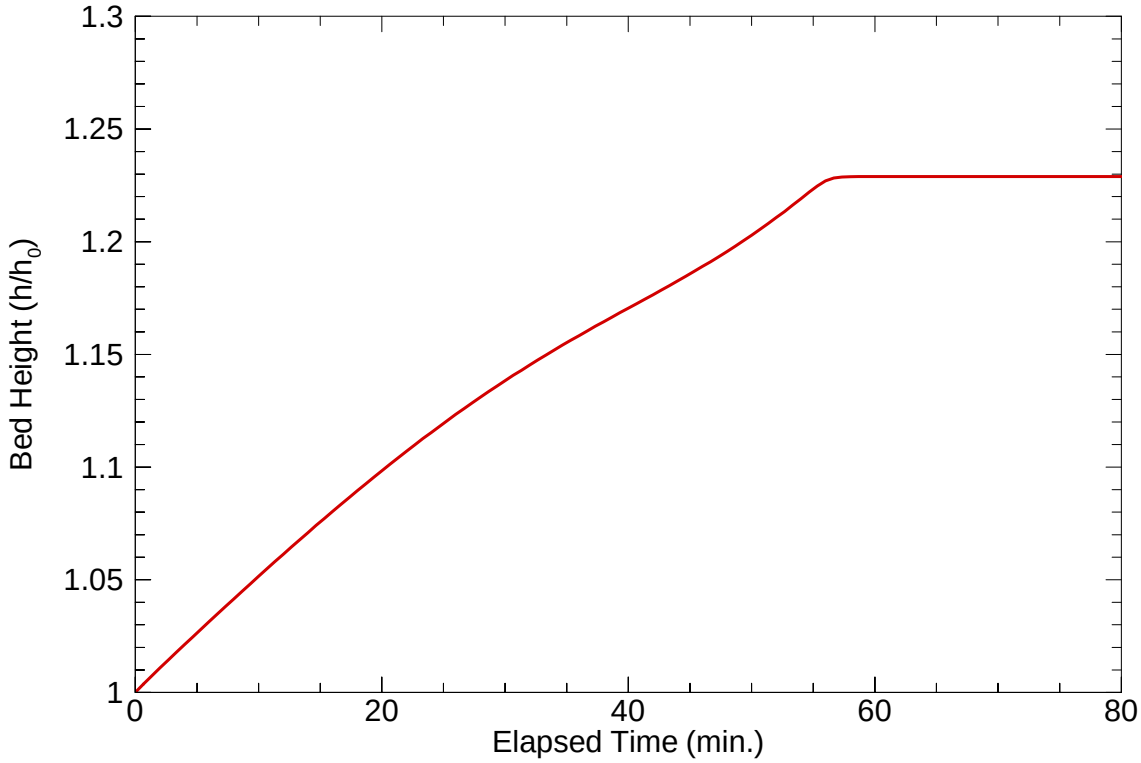

Fig. 7: Transient Bed Height.

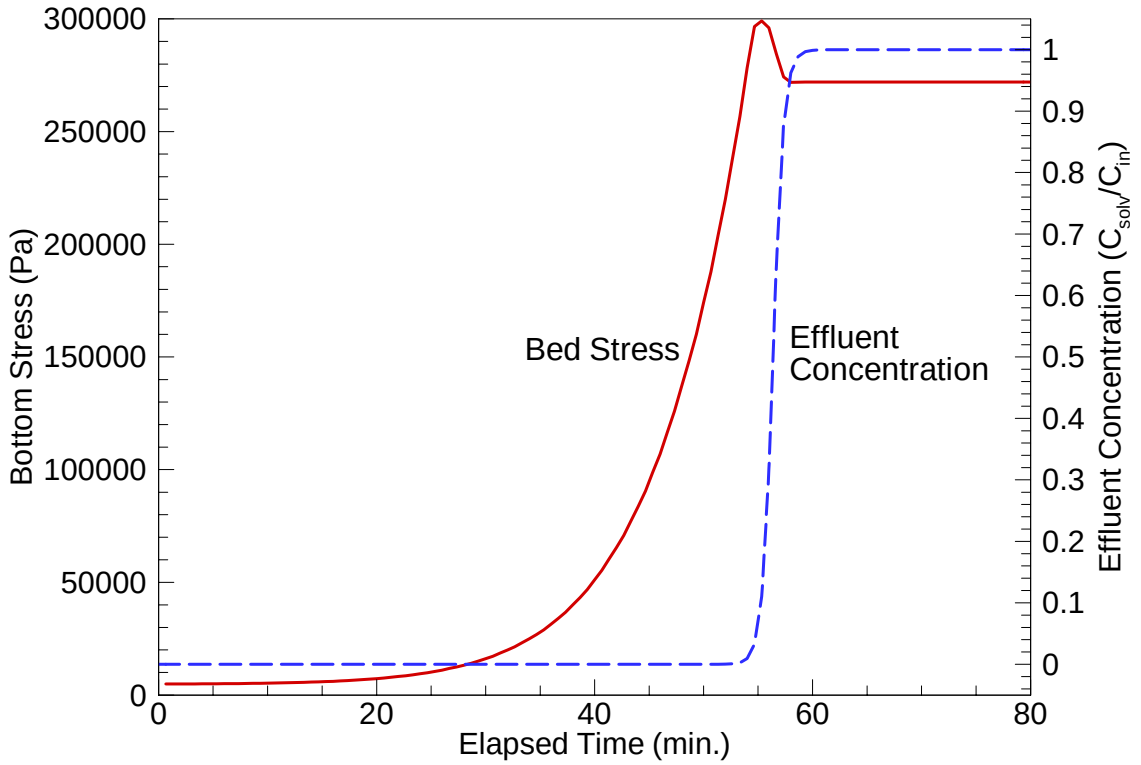

Fig. 8: Transient column bottom bed stress and effluent ion concentration.

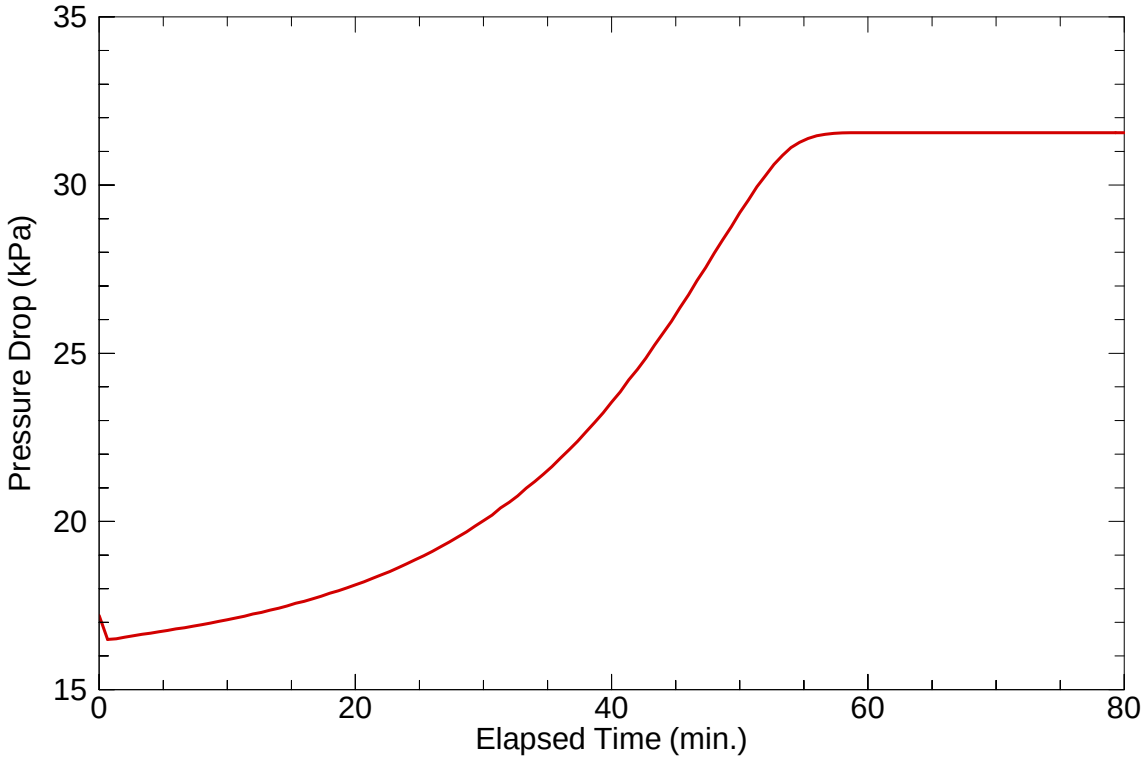

Fig. 9: Transient hydraulic pressure drop.

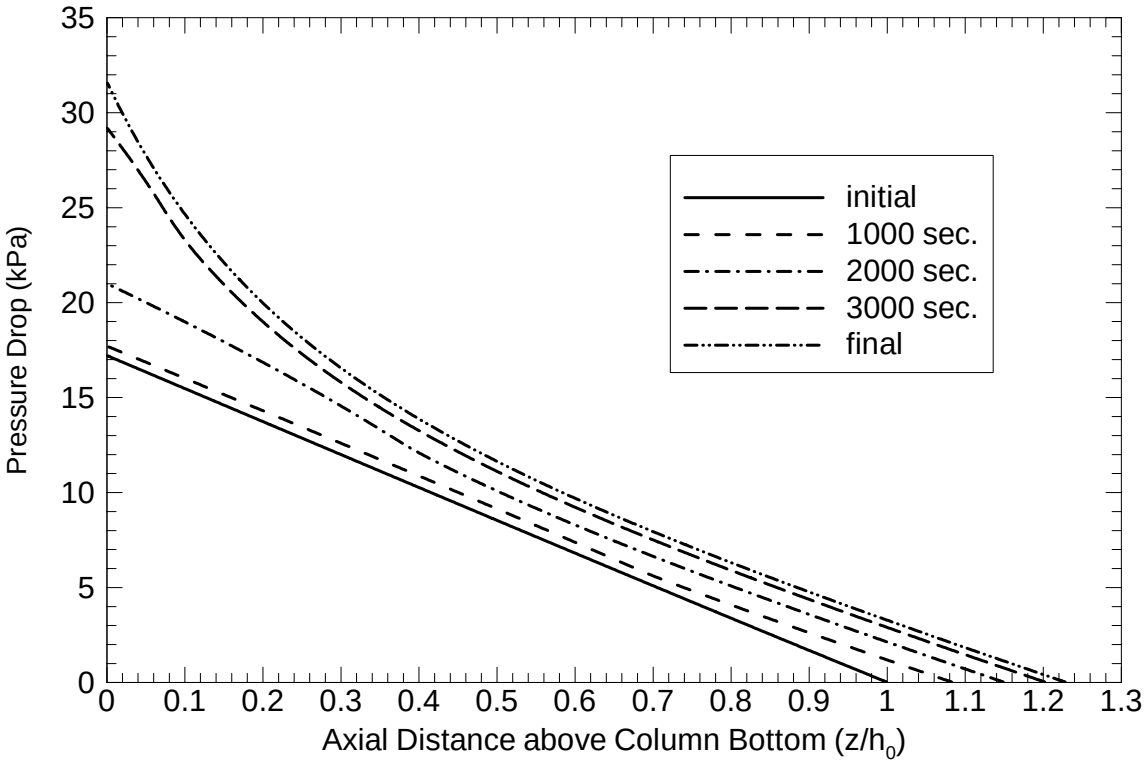

Fig. 10: Axial profiles of bed hydraulic pressure drop at five elapsed times during the transient.

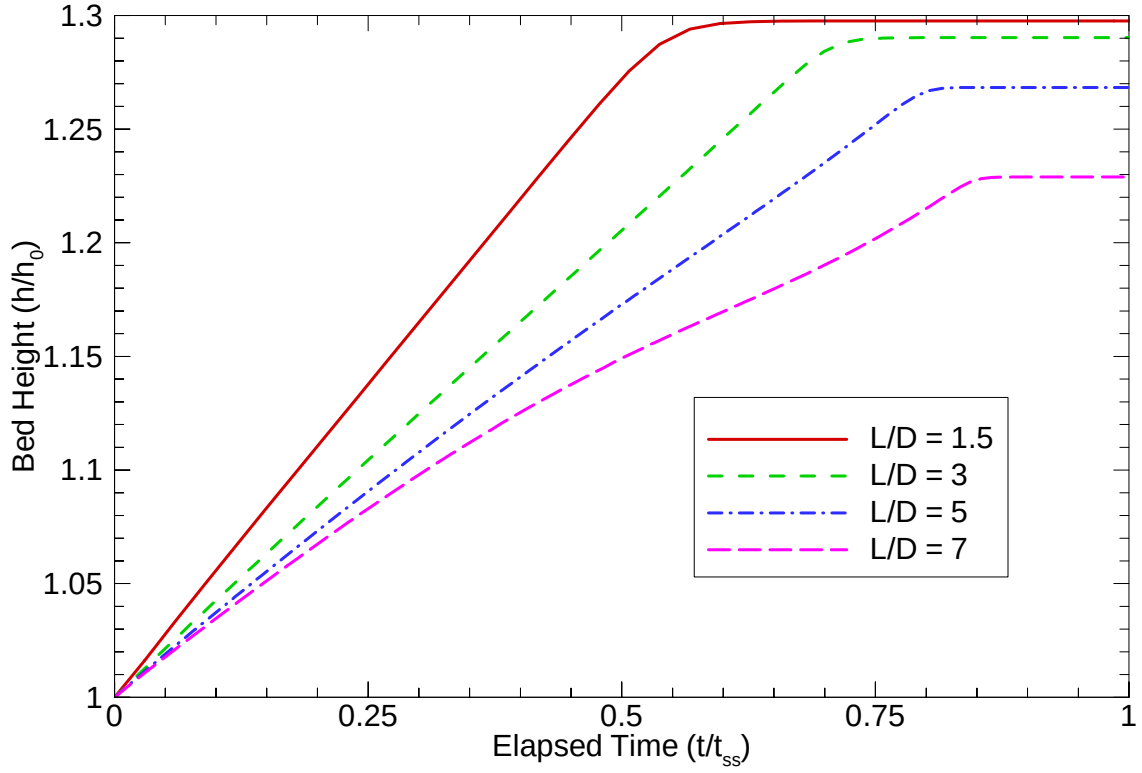

Fig. 11: Transient bed heights for a column with a diameter of 0.1 m. Results are shown for four values of the length to diameter ratio.

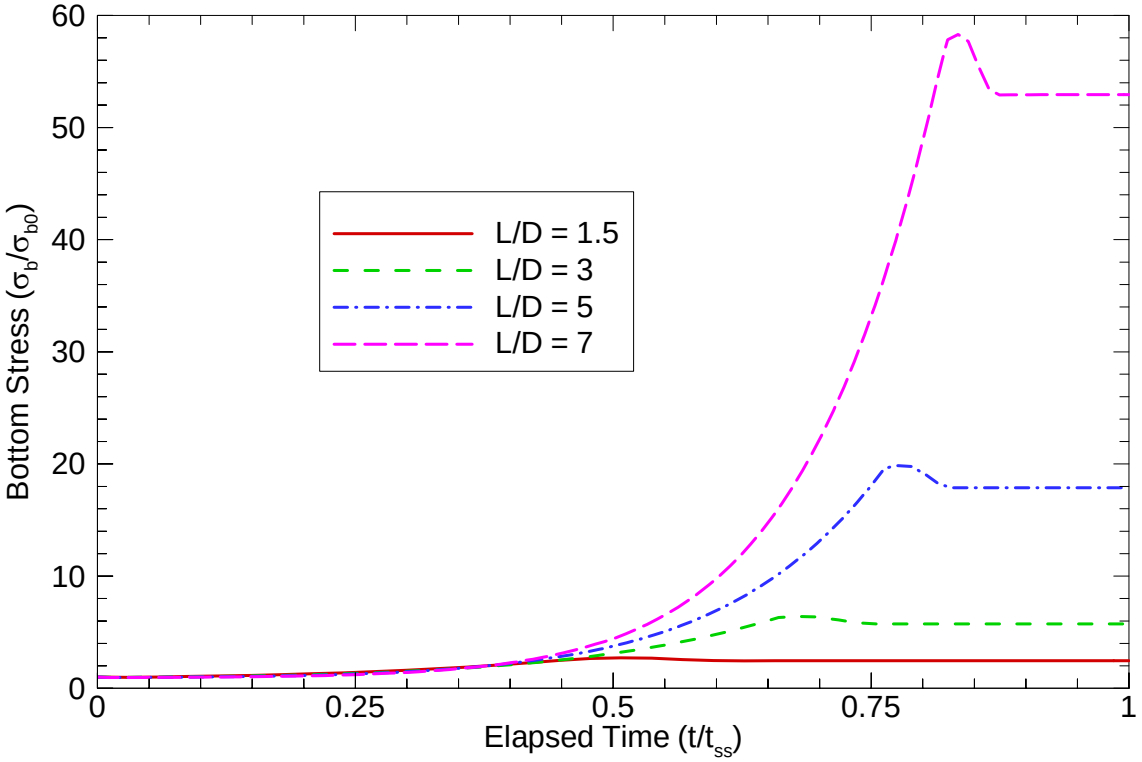

Fig. 12: Transient normalized bottom stress for a column with a diameter of 0.1 m. Results are shown for four values of the length to diameter ratio.

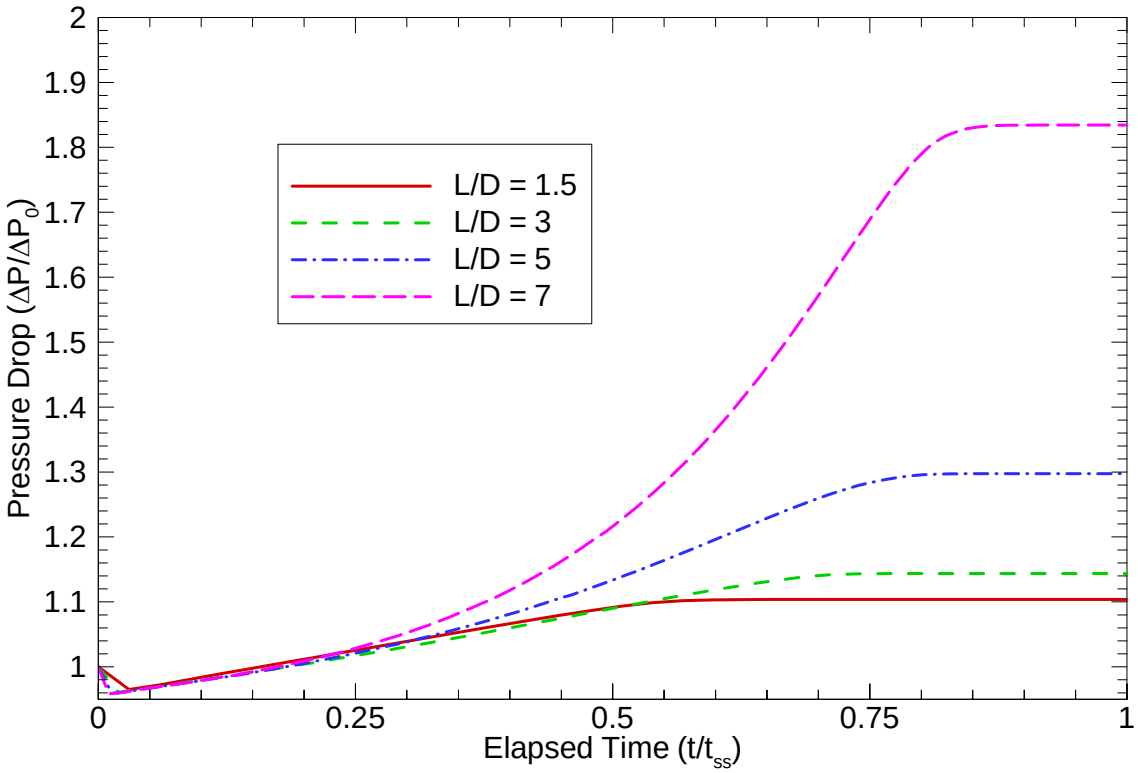

Fig. 13: Transient hydraulic pressure drops for a column with a diameter of 0.1 m. Results are shown for four values of the length to diameter ratio.

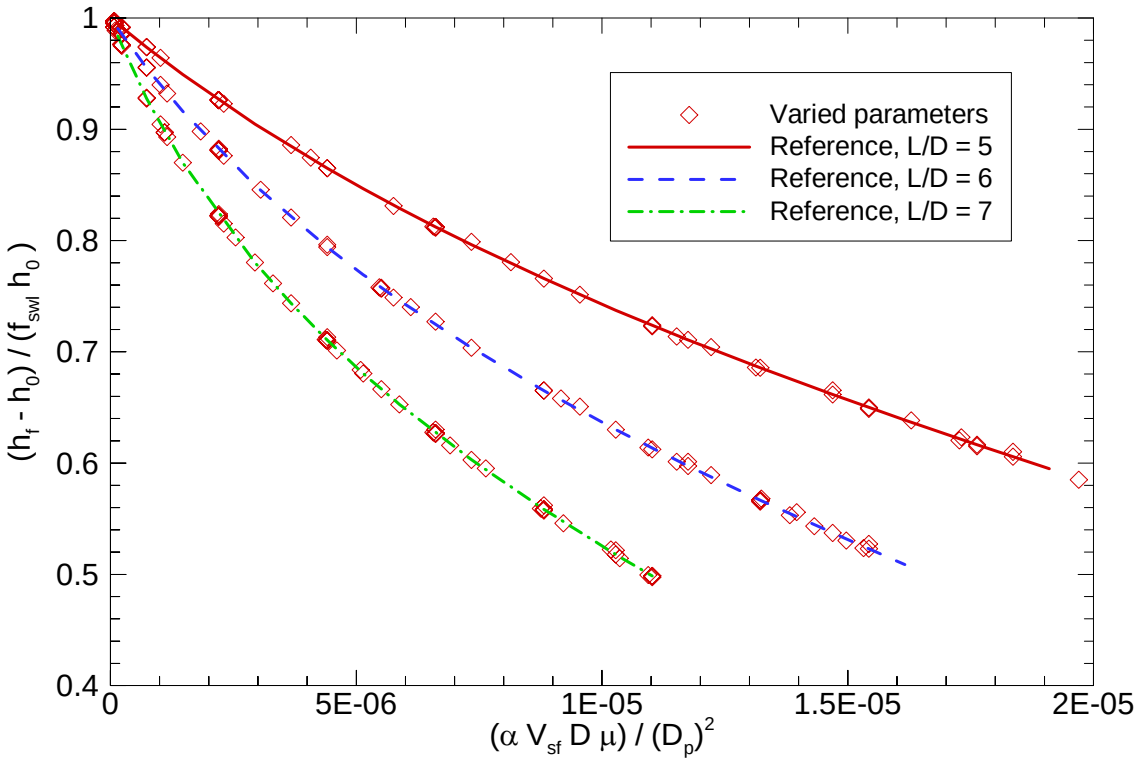

Fig. 14: Normalized final column height vs the non-dimensional resin compressibility $\bar{\alpha}$. The reference columns have diameters of 0.1 m. Results are shown for three values of the L/D ratio.

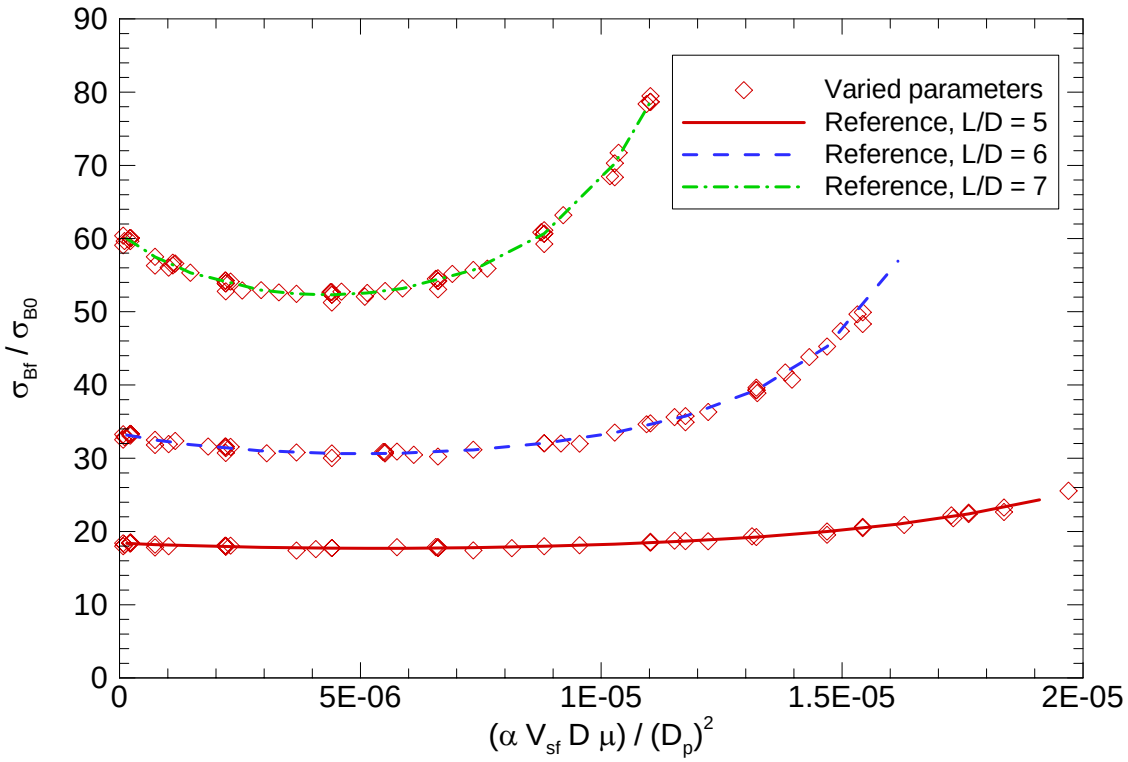

Fig. 15: Normalized final bottom bed stress vs the non-dimensional resin compressibility $\overline{\alpha}$. The reference columns have diameters of 0.1 m. Results are shown for three values of the L/D ratio.

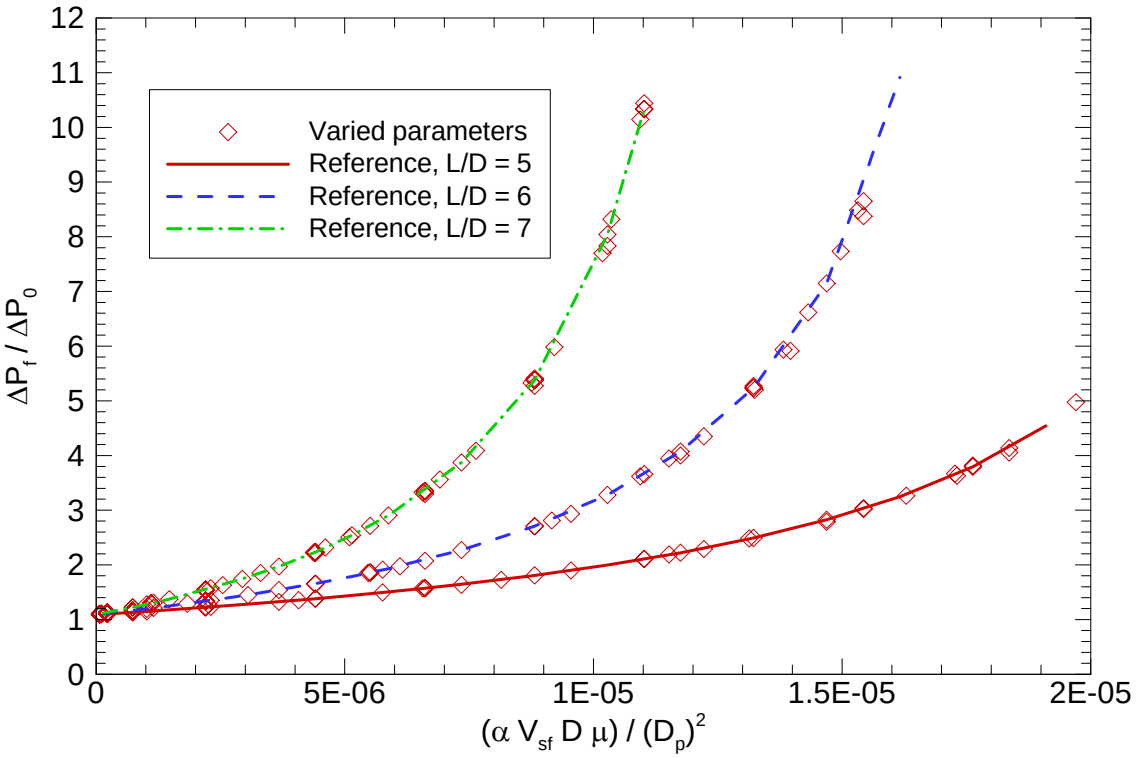

Fig. 16: Normalized final pressure drop vs the non-dimensional resin compressibility $\overline{\alpha}$. The reference columns have diameters of 0.1 m. Results are shown for three values of the L/D ratio.

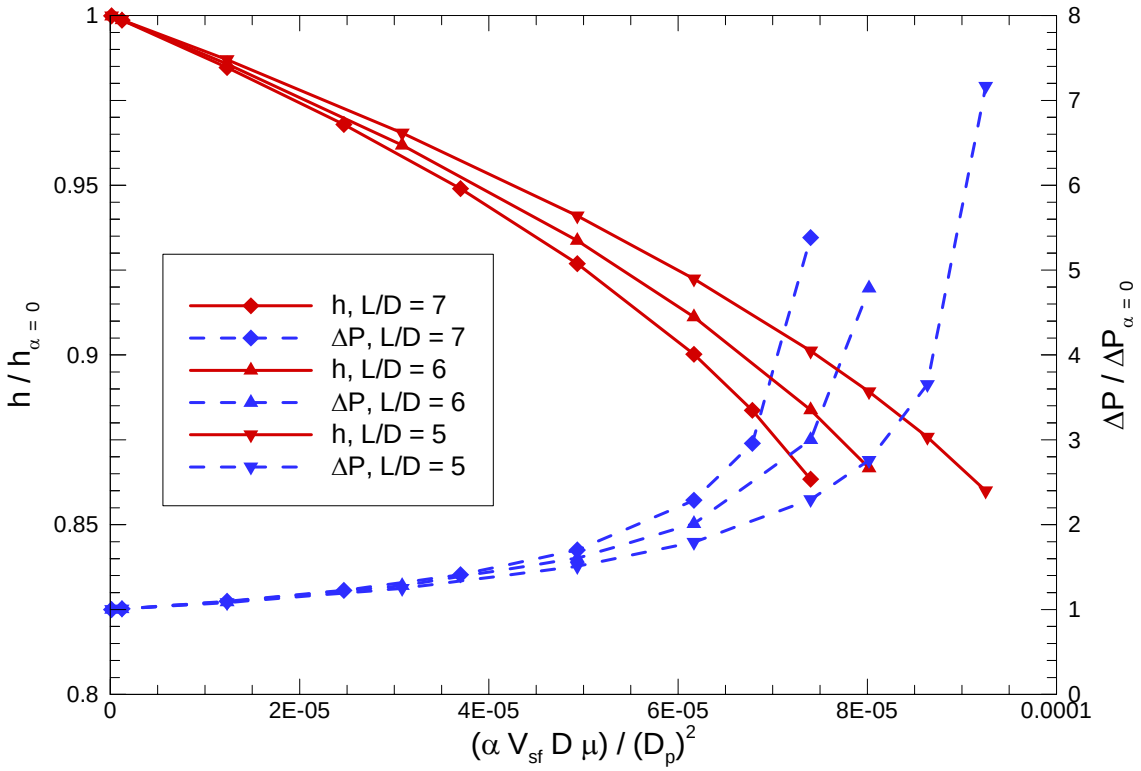

Fig. 17: Normalized column height and pressure drop vs the non-dimensional resin compressibility $\overline{\alpha}$ for steady flow. Results are shown for three values of the L/D ratio.